American Mineralogist, Volume 81, pages 1425–1437, 1996

Thermodynamics of order-disorder in minerals: II. Symmetric formalism applied to solid solutions

TIM HOLLAND[1] AND ROGER POWELL[2]

[1]Department of Earth Sciences, University of Cambridge, Cambridge CB2 3EQ, U.K.
[2]School of Earth Sciences, University of Melbourne, Victoria 3052, Australia

ABSTRACT

The thermodynamics of order-disorder in mineral solid solutions are handled with symmetric formalism, whereby the mineral is treated as a solid solution between an independent set of end-members with which the range of composition and states of ordering of the phase can be represented. An n-component mineral, requiring s independent order parameters to represent the state of order in the mineral, involves an independent set of $n + s$ end-members. Symmetric formalism involves ideal mixing-on-sites with regular-solution activity coefficients. It is applied to omphacite, orthopyroxene, ferromagnesian clinoamphibole, and alkali feldspar. The model for omphacite, with a single order parameter, successfully produces the topology of paired miscibility gaps with tricritical points at their apices and with a critical curve connecting them. Ferromagnesian orthopyroxene is shown to behave effectively as an ideal solution at all geologically relevant temperatures. Cummingtonite-grunerite solid solutions are slightly positively nonideal in either a two-site or a three-site model. Na-K alkali feldspars with order-parameter coupling involving tetrahedral site occupancies can show the essential topologic relationships in this system, with only one independent binary interaction energy. The power of symmetric formalism comes from the simplicity of its representation of the thermodynamics of minerals and its flexibility with few adjustable parameters.

INTRODUCTION

The increasing availability, in both quality and quantity, of standard-state thermodynamic properties of mineral end-members cannot result in a similar increase in accurately calculated phase equilibria until the mixing properties of complex solid solutions can be modeled more reliably. The traditional approach of taking all the nonideality into a heat-of-mixing term has worked adequately for phases that can be shown to be largely disordered, and this treatment of nonideality forms the basis of modern thermobarometry. However, many phases undergo progressive cation disordering with increasing temperature, and these effects are generally ignored or are treated by making the model heats of mixing temperature dependent. However, the behavior of disordering systems involves simultaneous and correlated changes in both the entropy and enthalpy with composition and temperature. The strong composition dependence of ordering typical of such phases is not handled by adding a temperature dependence to the heat of mixing. Two models currently in common use, which can handle the temperature and composition dependence of disordering, are the Landau theory (e.g., Carpenter et al. 1994; Carpenter and Salje 1994) and generalized Bragg-Williams models (e.g., Davidson and Burton 1987; Ghiorso 1990a, 1990b; Ghiorso et al. 1995).

A solid solution of n components involving no cation ordering requires n end-members, and $n - 1$ independent composition parameters, to represent all possible composition variations in the solid solution. To extend this treatment to handle order-disorder requires only that the order parameters be represented by additional end-members. For an n-component system with s independent order parameters, $n + s$ end-members are needed to represent all possible composition and order variations in the solid solution. For such a solid solution any of a variety of mixing models can be chosen to handle the mixing between the $n + s$ end-members. The equilibrium state of order is determined in this $(n + s)$-component fictive system, and this is then incorporated into the thermodynamic description.

The simplest model that can introduce the necessary degree of composition-dependent ordering involves ideal mixing on sites in combination with the regular-solution model: symmetric formalism of Powell and Holland (1993). A more complex approach could be adopted equally well, for example, using the subregular-solution model, if it should seem justified by the experimental data. However, symmetric formalism allows a considerable range of order-disorder phenomena to be modeled, with no particular constraint from the number of components or the number of order parameters. Treating a phase showing order-disorder as an $(n + s)$-component fictive system, with the use of symmetric formalism, is a

0003–004X/96/1112–1425$05.00

macroscopically derived equivalent to generalized Bragg-Williams models.

The purpose of this paper is to extend symmetric formalism, developed in Powell and Holland (1993) and applied to phases of fixed composition in the companion paper (Holland and Powell 1996), to cation ordering in solid solutions. The approach is illustrated using four mineral solid solutions: omphacite, involving convergent ordering to form a 1:1 compound in $NaAlSi_2O_6$-$CaMgSi_2O_6$; orthopyroxene, involving nonconvergent ordering on two sites in $MgMgSi_2O_6$-$FeFeSi_2O_6$; clinoamphibole, involving nonconvergent ordering on three sites in $Mg_3Mg_2Mg_2Si_8O_{22}(OH)_2$-$Fe_3Fe_2Fe_2Si_8O_{22}(OH)_2$; and alkali feldspar, involving order-parameter coupling in $NaAlSi_3O_8$-$KAlSi_3O_8$.

Order-disorder in a two-site mineral

The thermodynamic properties in symmetric formalism for a binary phase involving two-site ordering are outlined for use in the following sections. Such a phase constitutes a fictive ternary system because one order parameter is needed to describe its state of order. Consider that the formulas of the end-members of the phase involve two elements, A and B, mixing on m sites of M1 and n sites of M2. The three end-members used to describe such a system can be chosen to be $a = A_mA_n$, $b = B_mB_n$, and, for the ordered end-member, $o = A_mB_n$. Assuming that B prefers M2, the order parameter can be defined as $Q = x_B^{M2} - x_B^{M1}$. Thus, order can vary from complete disorder at $Q = 0$ to complete order at $Q = [(m + n)/n]X$ for $X < n/(m + n)$ and $Q = [(m + n)/m](1 - X)$ for $X > n/(m + n)$, with X the bulk composition in terms of B.

The site fractions are

$$\begin{aligned} x_A^{M1} &= 1 - X + \frac{n}{m+n}Q \\ x_B^{M1} &= X - \frac{n}{m+n}Q \\ x_A^{M2} &= 1 - X - \frac{m}{m+n}Q \\ x_B^{M2} &= X + \frac{m}{m+n}Q. \end{aligned} \tag{1}$$

The bulk composition, X, can be written as $X = [m/(m + n)]x_B^{M1} + [m/(m + n)]x_B^{M2}$. The proportions (or mole fractions) of the end-members are

$$\begin{aligned} p_a = x_A^{M2} &= 1 - X - \frac{m}{m+n}Q \\ p_b = x_B^{M1} &= X - \frac{n}{m+n}Q \\ p_o = x_B^{M2} - x_B^{M1} &= Q. \end{aligned} \tag{2}$$

The ideal mixing-on-sites activities (e.g., Wood and Banno 1973; Powell 1978; Anderson and Crerar 1993) are

$$\begin{aligned} a_a^{ideal} &= (x_A^{M1})^m(x_A^{M2})^n = (1 - p_b)^m p_a^n \\ a_b^{ideal} &= (x_B^{M1})^m(x_B^{M2})^n = p_b^m(1 - p_a)^n \\ a_o^{ideal} &= (x_A^{M1})^m(x_B^{M2})^n = (1 - p_b)^m(1 - p_a)^n \end{aligned}$$

and the regular-solution (e.g., Thompson 1967; Anderson and Crerar 1993) activity coefficients are

$$\begin{aligned} RT \ln \gamma_a &= (1 - p_a)p_bW_{ab} + (1 - p_a)p_oW_{ao} - p_bp_oW_{bo} \\ RT \ln \gamma_b &= p_a(1 - p_b)W_{ab} - p_ap_oW_{ao} + (1 - p_b)p_oW_{bo} \\ RT \ln \gamma_o &= -p_ap_bW_{ab} + p_a(1 - p_o)W_{ao} + p_b(1 - p_o)W_{bo}. \end{aligned} \tag{3}$$

The W_{ij} parameters are the macroscopic interaction energies for the i-j binaries. In a strictly atomistic interpretation, these would correspond to combinations of within-site and cross-site terms (see Powell and Holland 1993). However, although these macroscopic interaction energies can be derived on an atomistic basis, they may also include further contributions to the nonideal mixing, such as strain or other nonconfigurational energies.

The preceding development has been just that of the classical regular solution for a ternary system, but the equilibrium state of order must now be superimposed on this. This can be accomplished by making the first derivative of the Gibbs energy, G, equal to zero with respect to Q at constant X (as required at equilibrium), or, as shown in Appendix 1, by writing the equilibrium relationship for the internal reaction between the end-members, $ma + nb = (m + n)o$. This gives, on collection of terms

$$0 = A + BQ + CX + mnRT \ln K_D \tag{4}$$

in which

$$K_D = \frac{x_A^{M1}x_B^{M2}}{x_B^{M1}x_A^{M2}} = \frac{(1 - p_a)(1 - p_b)}{p_ap_b} \tag{5}$$

and

$$\begin{aligned} A &= \Delta H_R^0 + (m + n)W_{ao} - nW_{ab} \\ B &= \frac{2}{m+n}[-m^2W_{ao} + mn(W_{ab} - W_{ao} - W_{bo}) - n^2W_{bo}] \\ C &= m(W_{bo} - W_{ao} - W_{ab}) + n(W_{bo} - W_{ao} + W_{ab}). \end{aligned} \tag{6}$$

In such a fictive ternary system only three adjustable parameters, A, B, and C, are involved in representing order as a function of temperature and composition. The values of these parameters control the order-disorder behavior of the system as follows:

(1) If $C = 0$ and $W_{bo} = W_{ao}$, then the thermodynamic properties (order parameter, enthalpy, volume, entropy, and heat capacity) of the binary are symmetric about $X = 0.5$. If C is nonzero, certain properties of the binary, such as enthalpy of mixing, can be quite asymmetric.

(2) If $A + CX = 0$, the system is convergent, as in the classical Bragg-Williams model, and for stability B must be negative. In such a case there is a critical temperature,

T_c, above which the phase is completely disordered and below which the degree of order increases sharply with decreasing temperature. It is found by solving the equilibrium relation (Eq. 4) for temperature in the limit as $Q \rightarrow 0$:

$$T_c = -\frac{BX(1 - X)}{Rmn}. \quad (7)$$

T_c has a maximum value at $X = 0.5$. Convergent ordering generally accompanies a phase transition, in which a change in space group symmetry occurs between the high-temperature disordered form and the low-temperature ordered form.

(3) If $B = 0$ and $C = 0$, the model reduces to the simple disordering model used by Navrotsky (1971) and Molin et al. (1991) for ferromagnesian orthopyroxene. This situation might result when either all interaction energies are equal to zero or $W_{ab} = 2(W_{ao} + W_{bo})$. Although possible in principle, the latter is unlikely to be a common situation.

(4) The sum $A + CX$ can only be zero or a negative value for stability (otherwise the anti-ordered end-member, $B^{M1}A^{M2}$, would be more stable than o). $A + CX$ is referred to as the field because it expresses an energy acting like an applied field that prevents the two sites from becoming identical (converging) in their energetic states. The presence of a field characterizes nonconvergent ordering, which typically occurs in phases that undergo continuous disordering with no change in space group symmetry and hence no phase transition to a higher symmetry form.

In addition, the enthalpy of mixing, entropy of mixing, volume of mixing, and heat capacity can be formulated for the symmetrical formalism model (see Appendix 2).

Ordering in omphacite

Omphacite is the name given to ordered (space group $P2/n$) pyroxene at intermediate compositions along the $NaAlSi_2O_6$-$CaMgSi_2O_6$ join. Disordered high-temperature clinopyroxene has space group $C2/c$, and the onset of ordering below $T_c = 860$ °C (Carpenter 1981) is driven by partitioning of Mg and Al onto separate M1a and M1b sites, which were equivalent above the critical temperature. The M2 sites also split into M2a and M2b, between which Na and Ca order below T_c. The thermodynamics of omphacite ordering have been investigated in terms of generalized Bragg-Williams models (Davidson and Burton 1987) and by Landau theory (Carpenter et al. 1990; Holland 1990). Because of the charge-balanced substitution CaMg-NaAl, the ordering on M2 is not independent of that on M1, and the system of four split half-sites (M1a, M1b, M2a, M2b) can be considered energetically as equivalent to ordering of a pair of cations on two sites. This simple assumption is corroborated by (1) the finding of Carpenter et al. (1990) that the order parameter for M2 is linearly dependent on that for M1, and (2) that for convergent omphacite both order parameters must be zero at T_c. Thus, in what follows, we treat omphacite as an example of an ordered compound in a binary solid solution.

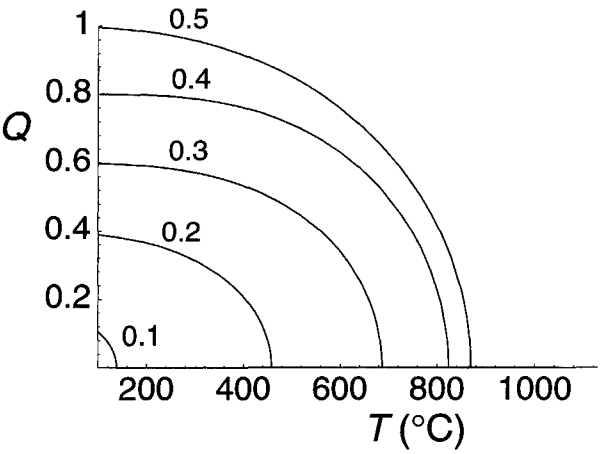

FIGURE 1. Order parameter Q vs. T, with contours of composition, X, for the diopside-jadeite binary.

Consider the end-members, diopside d, jadeite j, and the ordered end-member o. The state of order can be represented by an order parameter, Q, defined as $Q = X_{Al}^{M1a} - X_{Al}^{M1b}$, and order can vary from complete disorder, $Q = 0$, to complete order, $Q = 2X$ for $X \leq ½$, and $Q = 2(1 - X)$ for $X \geq ½$, where X is the proportion of jadeite in the diopside-jadeite binary.

From the previous section, with $m = n = 1$, the equilibrium state of order as a function of composition and temperature in the d-j-o fictive ternary system is given by the equilibrium relationship for the reaction between the end-members, d + j = 2o:

$$0 = A + BQ + CX + RT \ln K_D \quad (8)$$

in which

$$A = \Delta H_R - W_{dj} + 2W_{do}$$
$$B = W_{dj} - 2(W_{do} + W_{jo})$$
$$C = 2(W_{jo} - W_{do}). \quad (9)$$

Assuming that the properties are symmetrical about $X = 0.5$, then $C = 0$. Furthermore, because omphacite disorders convergently, $A = 0$ because $A + CX$ must be zero. With the known value of $T_c = 1133$ K at $X = 0.5$, Equation 7 gives $B = -4RT_c$. Only one further piece of information is required to solve these relations for all the unknown interaction energies. The activity measurements of Holland (1983) and the calorimetry of Wood et al. (1980) give the value $W_{dj} = 26$ kJ. Therefore, $W_{dj} = 26$, $W_{do} = 16$, $W_{jo} = 16$, and $\Delta H_R = -6.0$ kJ. With the use of these data, the state of order can be calculated as a function of temperature and composition using Equation 4 (see Figs. 1 and 2). In the latter figure, the state of order is presented on a d-j-o triangle to emphasize the ternary nature of the system, with the fully disordered phase lying along the baseline ($p_o = 0$) and the fully ordered phase

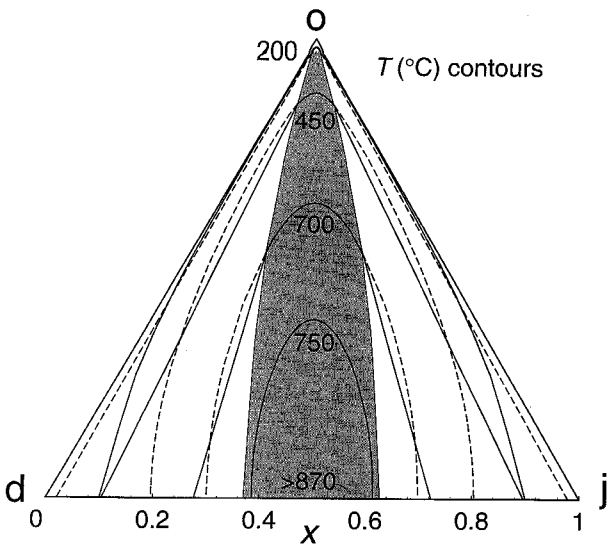

FIGURE 2. Order-disorder in the diopside-jadeite binary represented as a fictive ternary in terms of end-members jadeite, diopside, and omphacite, contoured for T.

lying at the om apex (p_o = 1). Calculated activities for the jadeite component at several temperatures are shown in Figure 3. The square root of the activity is plotted to show the effective one-site activity behavior (including adherence to Raoult's and Henry's laws at high and low values of X, respectively). Note the miscibility gaps and the extremely steep activity-composition slope near X = 0.5. The enthalpy of mixing, entropy of mixing, and heat capacity as a function of composition and temperature for this system are shown in Appendix 2.

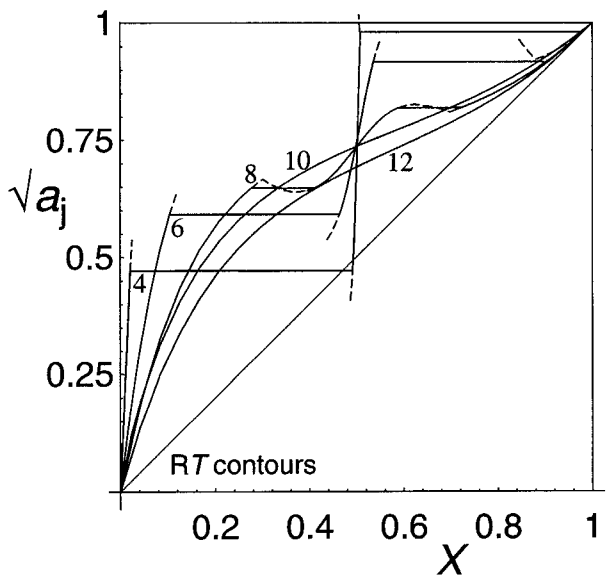

FIGURE 3. Activity-composition relationships (a-X) for the diopside-jadeite binary, contoured for RT (in kilojoules). The activity of jadeite is shown; the activity of diopside is identical following reflection across X = 0.5. The activity is shown as $\sqrt{a_j}$, so that ideal mixing is given by a line of unit slope. The horizontal lines are tie lines across the miscibility gaps.

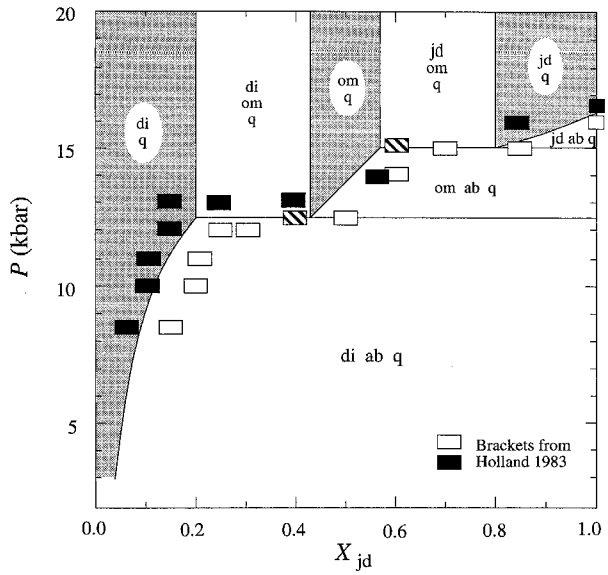

FIGURE 4. A P-X section for the system jadeite-diopside-quartz involving quartz, albite, and pyroxene (cpx) in the jadeite-diopside binary in projection from quartz at 600 °C. The experimental results are from Holland (1983); the open and solid symbols are reversed brackets of the cpx composition in the equilibrium [see Holland (1983) for details]. The section itself was produced with THERMOCALC (Powell and Holland 1988).

The close agreement of the simple model with the experimental results of Holland (1983) is illustrated in the P-X section of Figure 4. Some petrologic consequences of ordering in omphacite are illustrated in a calculated P-T diagram (Fig. 5), which shows three univariant reactions, jadeite + quartz = albite, jadeite$_{ss}$ + quartz = omphacite$_{ss}$ + albite, and omphacite$_{ss}$ + quartz = diopside$_{ss}$ + albite. The third reaction gives the minimum pressures for the stability of eclogitic rocks containing ordered omphacite + quartz. These equilibria were calculated with the use of a recent update of the thermodynamic data set of Holland and Powell (1990).

This system shows development of paired miscibility gaps at low temperatures, with tricritical points at their apices and the critical curve connecting them (Fig. 6). This occurs when there is a large positive enthalpy of mixing for the disordered solid solutions in the binary join coupled with a strong tendency to order at an intermediate composition. At high temperatures the solid solutions are homogeneous and disordered, whereas at low temperatures an ordered omphacite develops that is centered on the composition X = 0.5. This strong ordering tendency splits what might otherwise have been a broad simple solvus into the pair of miscibility gaps shown in Figure 6. The model here reproduces the topology proposed by Carpenter (1980) for the convergent ordering of omphacite.

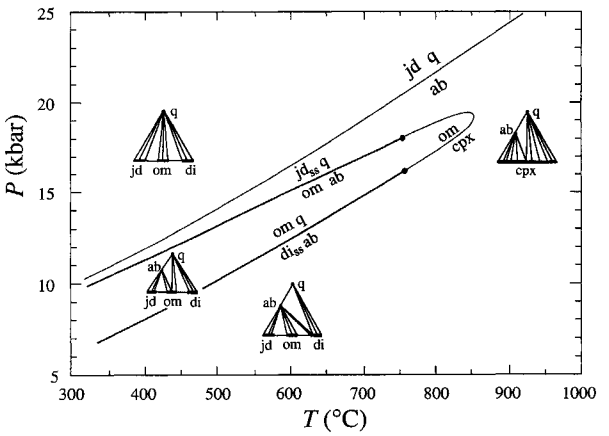

FIGURE 5. A calculated P-T diagram for the system jadeite-diopside-quartz in projection from quartz, produced with THERMOCALC and symmetric formalism description of the jadeite-diopside binary outlined in the text. The position of the jadeite + albite + quartz equilibrium is also shown. The om = cpx equilibrium marks the coexistence of omphacite, disordered cpx (Q = 0), albite, and quartz. Note that the state of order and the composition of the cpx vary along the equilibria.

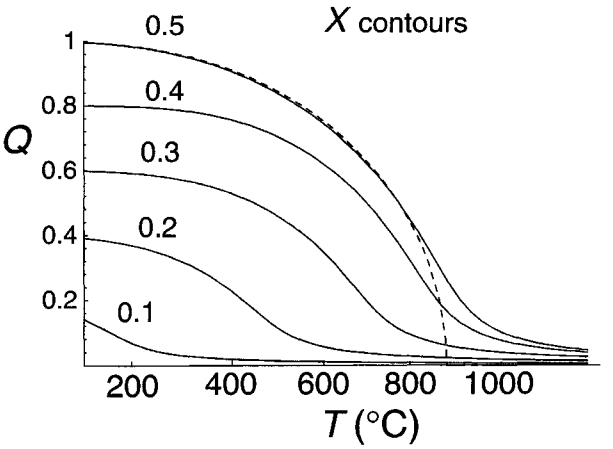

FIGURE 7. Order parameter Q vs. T, with contours of composition, X, for a nonconvergent system created from the diopside-jadeite binary (see text), using parameters such that the temperature for Q = 0.5 remains the same. See Figure 1 to compare with the convergent case.

Above, the convergent behavior of omphacite was discussed. With the addition of a small field, however, A is small and negative and the resulting mineral is nonconvergent. This smoothes the features associated with Q dropping to zero at the critical temperature, as can be seen in Figure 7. The order parameter drops to low values but never reaches zero even at very high temperatures. In a T-X diagram, certain ranges of parameter values also lead to paired miscibility gaps, but in contrast to the convergent case there is no phase transition, and hence no critical curve, and the solvus crests are rounded rather than cusp-peaked (Fig. 8).

NONCONVERGENT EXAMPLES: FERROMAGNESIAN ORTHOPYROXENE

The thermodynamics of nonconvergent ordering in orthopyroxene have been discussed extensively in the recent literature (e.g., Sack 1980; Chatillon-Colinet et al. 1983; Carpenter and Salje 1994; Sack and Ghiorso 1994; Kroll et al. 1994), and a wealth of experimental data on the ordering now exist (Saxena and Ghose 1971; Besancon 1981; Grammenopoulou 1981; Anovitz et al. 1988; Molin et al. 1991; Skogby 1992; Yang and Ghose 1994). Ferromagnesian orthopyroxene is represented by a fictive ternary system involving enstatite (en, $Mg_2Si_2O_6$), ferrosilite (fs, $Fe_2Si_2O_6$), and a fully ordered ferromagnesian pyroxene (fm, $FeMgSi_2O_6$) in which Fe prefers the M2 site over the M1 site. Parameters for use in Equation 4

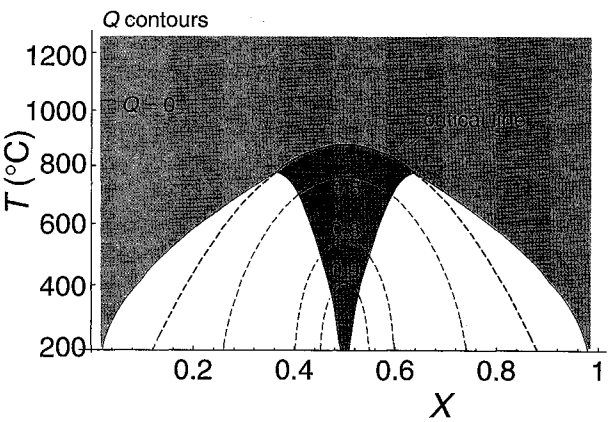

FIGURE 6. A T-X phase diagram for diopside-jadeite contoured for order parameter Q. The ordered phase (dark gray) is separated from the disordered (Q = 0) phase (light gray) by the critical line, at which Q goes to zero with increasing T. The solvi open at tricritical points on the critical line with decreasing T. T_c (at X = 0.5) is 860 °C.

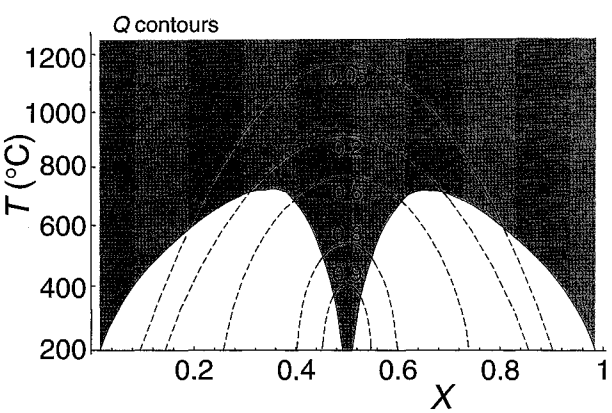

FIGURE 8. A T-X phase diagram for a nonconvergent system created from the diopside-jadeite binary (see text), contoured for order parameter Q. There is no critical line; Q decreases with increasing T but does not become zero at finite T. The solvi have rounded tops (compare Fig. 6).

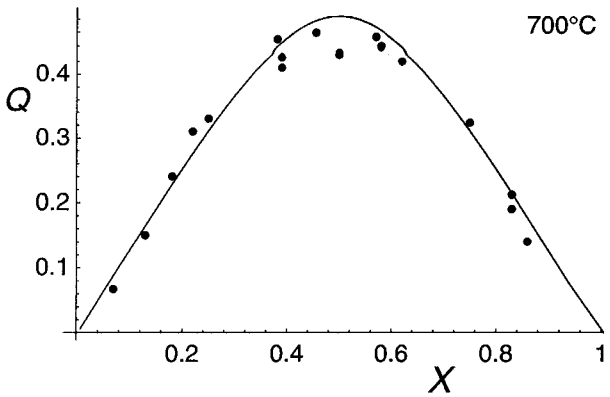

FIGURE 9. Order parameter $Q = x_{Fe}^{M2} - x_{Fe}^{M1}$ vs. X for experimental site-distribution data at 700 °C for orthopyroxene in comparison with the calculated Q-X line at this temperature obtained using the parameters produced by regression of all the data (see text).

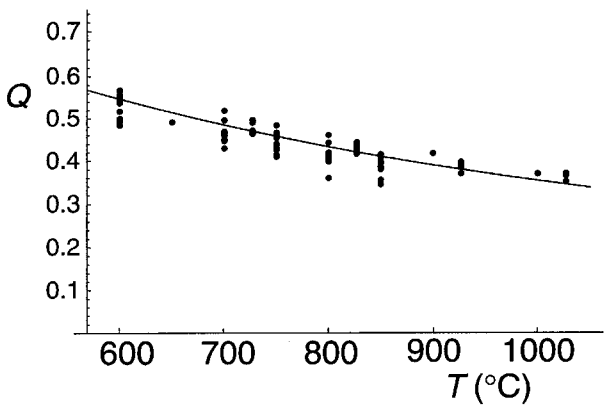

FIGURE 10. All the experimental site-distribution data for orthopyroxene plotted against T, projected to $X = 0.5$, in comparison with the calculated Q-T line for $X = 0.5$ obtained using the parameters produced by regression of the data (see text).

were derived by nonlinear regression of the values of $Q = X_{Fe}^{M2} - X_{Fe}^{M1}$ from the site-distribution data, yielding $A = -11.7$, $B = -11.2$ kJ, with $C = 0$ within error. This implies that $W_{en\,fm} = W_{fs\,fm}$. The individual interaction energies and the enthalpy, ΔH_R, for en + fs = 2 fm are determined from Equation 6

$$A = \Delta H_R - W_{en\,fs} + 2W_{en\,fm}$$

$$B = W_{en\,fs} - 2W_{en\,fm} - 2W_{fs\,fm} \qquad (10)$$

requiring at least one further piece of information. The possible constraint provided by the enthalpy-of-mixing measurement of 2.0 kJ at $X = 0.5$ and $Q = 0.3$ (Chatillon-Colinet et al. 1983) unfortunately yields interaction energies that are too large to satisfy the precise partitioning experiments of von Seckendorff and O'Neill (1993). These experiments provide a powerful constraint on the magnitude of the orthopyroxene energetics because the Fe-Mg interaction energy in olivine is well known. $W_{fo\,fa}$ is given as 4.0 kJ/atom, a compromise between the values of 3.7 ± 0.8 from Wiser and Wood (1991), 4.5 ± 1.0 from Hackler and Wood (1989), and 5 ± 3 from Figure 3 in the review of von Seckendorff and O'Neill (1993). The olivine-orthopyroxene partitioning experiments, combined with $W_{fo\,fa} = 4$ kJ and the constraints $A = -11.7$, $B = -11.2$ kJ, give $W_{en\,fs} = 6.8$, $W_{en\,fm} = 4.5$, $W_{fs\,fm} = 4.5$, and $\Delta H_R = -13.9$ kJ.

The results of the fitting of the experimental data are summarized using four figures: Figure 9 is a Q-X diagram indicating the appropriateness of the form of Equation 4 at constant temperature; Figure 10 is a Q-T diagram with all the experimental data projected to $X = 0.5$ to show the overall quality of fit to the data; Figure 11 shows the close fit to the olivine-orthopyroxene partitioning data of von Seckendorff and O'Neill (1993); and Figure 12 is an a-X diagram indicating that the calculated activities exhibit very little deviation from ideality at all petrologically applicable temperatures, confirming the conclusions reached by Chatillon-Colinet et al. (1983) and Perkins and Vielzeuf (1992). Without further phase-equilibrium or intercrystalline partitioning constraints such as the data of von Seckendorff and O'Neill (1993), orthopyroxene could be made to have quite large nonideality within the limits provided by Equation 10. If the magnitude of $W_{en\,fm}$ were made a little larger (e.g., 6.8 kJ), then the magnitude of $W_{en\,fs}$ would become rather large (15.5 kJ) and thus propagate to much larger calculated nonideality.

FERROMAGNESIAN CLINOAMPHIBOLE

The ferromagnesian clinoamphibole cummingtonite-grunerite, $(Fe,Mg)_7Si_8O_{22}(OH)_2$, exhibits ordering on at least three separate sites: M2, M4, and a combined M1 + M3 site (M13), with $X_{Fe,M4} \gg X_{Fe,M13} > X_{Fe,M2}$ (Hirschmann et al. 1994). The partitioning between M4 and M2 is quite pronounced, but that between M2 and M13 is much less so. The high-low cummingtonite phase transition, which occurs at quite low temperatures, probably contributes little to the energetics of the system and is ignored in this study. The thermodynamics of this system have been extensively analyzed using the generalized Bragg-Williams model by Ghiorso et al. (1995) and Evans and Ghiorso (1995). The approach here is entirely equivalent to the three-site and two-site models used by Ghiorso et al. (1995) but with symmetric formalism providing a very compact and simple representation of the same information. To deal with ordering on three sites, two ordered end-members are required in addition to the binary end-members cummingtonite (c, $Mg_3Mg_2Mg_2$) and grunerite (g, $Fe_3Fe_2Fe_2$), and the pair a ($Mg_3Fe_2Fe_2$) and b ($Fe_3Mg_2Fe_2$) is adopted in terms of sites M13, M2, and M4. In this solid solution two order parameters are needed, for example $Q_1 = X_{Fe}^{M4} - X_{Fe}^{M13}$ and $Q_2 = X_{Fe}^{M4} - X_{Fe}^{M2}$. They are determined by solving the equilibrium relationships for the two independent reactions

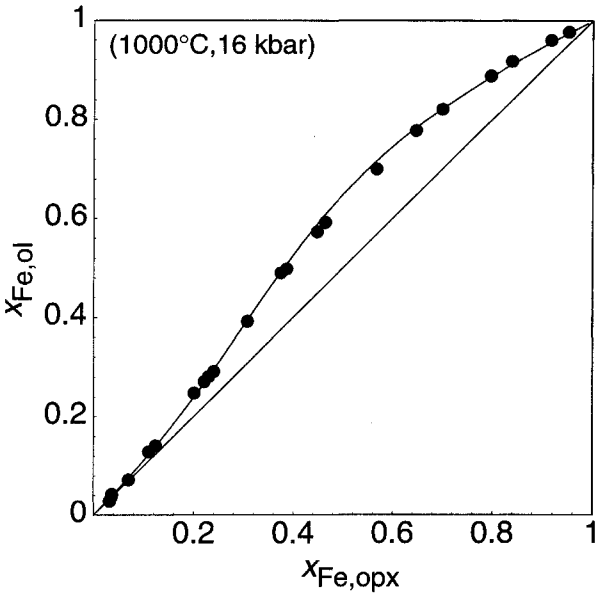

FIGURE 11. Ferromagnesian partition between olivine and orthopyroxene at 1000 °C. The curve calculated using symmetric formalism of this study is compared with the experimental data (solid circles) of von Seckendorff and O'Neill (1993).

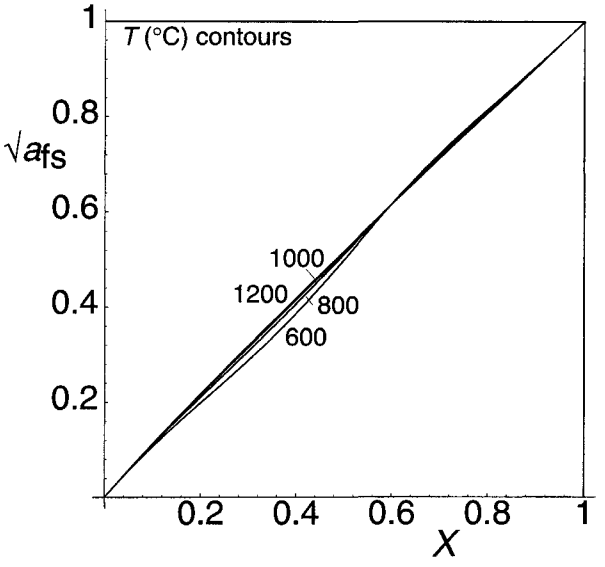

FIGURE 12. Calculated activity-composition relationships for orthopyroxene at a series of temperatures, in terms of the square root of the activity of ferrosilite; the activity of enstatite is the mirror image reflected across $X = 0.5$. The proximity to a 1:1 line shows that orthopyroxene is effectively ideal in this temperature range, in agreement with Perkins and Vielzeuf (1992).

$$3c + 4g = 7a$$
$$2c + 5g = 7b. \quad (11)$$

The experimental data of Hirschmann et al. (1994) suggest that the equilibrium constants for the above reactions do not depend on X, and so the analogs of the C term in Equation 4 are zero. For each of the above reactions there is a relationship, like Equation 4, found from substituting the activities into the equilibrium condition, giving

$$0 = A_1 + B_{11}Q_1 + B_{12}Q_2 + RT \ln K_1$$
$$0 = A_2 + B_{21}Q_1 + B_{22}Q_2 + RT \ln K_2 \quad (12)$$

in which the C terms have been set to zero. The subscripts 1 and 2 correspond to the first and second reactions written above. The parameters, in terms of the interaction energies are, for the first reaction

$$A_1 = \Delta H_1 + 7W_{cb} - 5W_{cg}$$
$$B_{11} = 7W_{cg} - 2W_{ca} - 3W_{cb} + \frac{23}{7}W_{cg} - 5W_{ga} - 4W_{gb}$$
$$B_{12} = \frac{20}{7}W_{cg} - 4W_{cb} - 10W_{gb} \quad (13)$$

and for the second reaction

$$A_2 = \Delta H_2 + 7W_{ca} - 4W_{cg}$$
$$B_{21} = \frac{24}{7}W_{cg} - 6W_{ca} - 8W_{ga}$$
$$B_{22} = B_{11}. \quad (14)$$

Unfortunately, as in the orthopyroxene case above, the site-partitioning data alone are not sufficient to determine the five separate parameters by regression, so the following assumptions were made to reduce the number of free parameters: $W_{ga} = 3W_{M13} = 13.5$ kJ, $W_{gb} = 2W_{M2} = 9$ kJ, and $W_{cg} = 3W_{M13} + 2W_{M2} + W_{M13,M2} = 22.5$ kJ were determined on the basis that a typical value for the regular-solution parameter for Fe-Mg mixing on an octahedral site is approximately 4.5 kJ (as in orthopyroxene), and that the cross-site term between M13 and M2 is zero. With these assumptions, the site-distribution data of Hirschmann et al. (1994) were regressed to yield values for $A_1 = -94.4$, $A_2 = -88.4$, and $W_{cg} = 39.8$. Substitution of these assumptions and constraints gives the remaining unknowns: $\Delta H_1 = -77.8$, $\Delta H_2 = -63.5$, $W_{ca} = 19.2$, and $W_{cb} = 26.1$ kJ.

The variation of the order parameters with composition at 700 °C is shown in Figure 13, illustrating the close agreement with the site-distribution experiments. Figure 14 shows the interrelation of Q_1 and Q_2 on a Q_1-Q_2 plot at several temperatures. Finally, the calculated activities of grunerite are shown in Figure 15 for several temperatures. The variation with temperature is not great, and the activities show a small positive departure from ideality at all geologically relevant temperatures. The activity of cummingtonite, if plotted, would show identical behavior because the solid solution is assumed to be symmetrical. As with orthopyroxene, more nonideal mixing than is shown in Figure 15 can be obtained with a larger value of Ws, while maintaining consistency with the site distributions.

Because the partitioning of Fe-Mg between M2 and

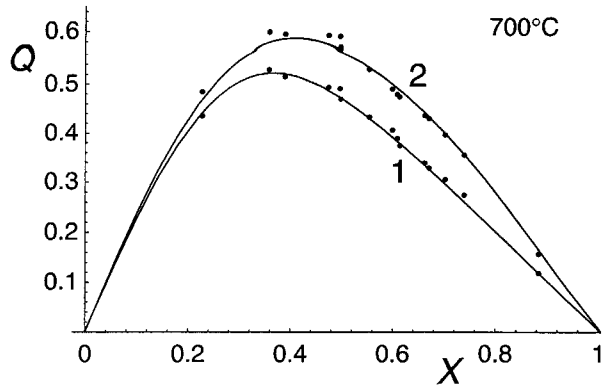

FIGURE 13. Order parameters $Q_1 = x_{Fe}^{M4} - x_{Fe}^{M13}$ and $Q_2 = x_{Fe}^{M4} - x_{Fe}^{M2}$ vs. X for the experimental site-distribution data of Hirschmann et al. (1994) at 700 °C for cummingtonite-grunerite in comparison with the calculated Q_1-X and Q_2-X lines at this temperature obtained using the parameters produced by regression of all the data (see text).

M13 is minor in comparison with that between either of these sites and M4 (Hirschmann et al. 1994), it transpires that a much simpler model involving just two effective kinds of sites, two M4 and five M123 sites, can fit the data satisfactorily and yield virtually identical activity-composition relationships. Ghiorso et al. (1995) referred to this as their two-site reduction. A single-ordered end-member Fe_2Mg_5 (d) is used together with cummingtonite (c) and grunerite (g) in a fictive ternary solution. In the equilibrium condition for the internal reaction 5c + 2g = 7d from Equation 6

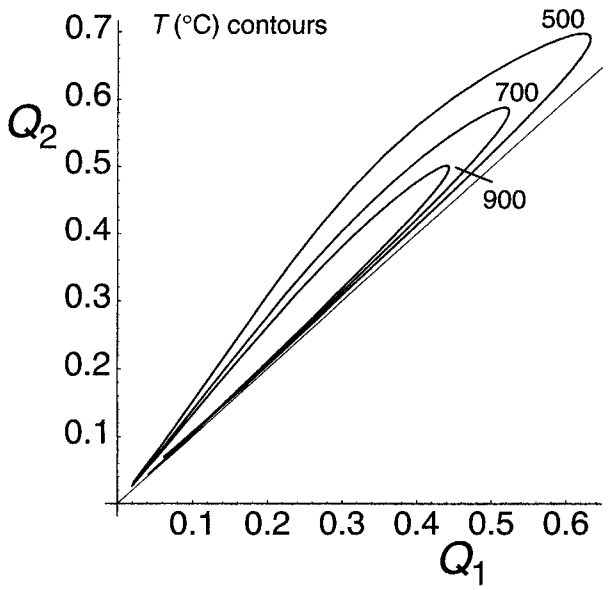

FIGURE 14. A calculated Q_1 vs. Q_2 diagram for a series of temperatures, using the parameters produced by regression of the data.

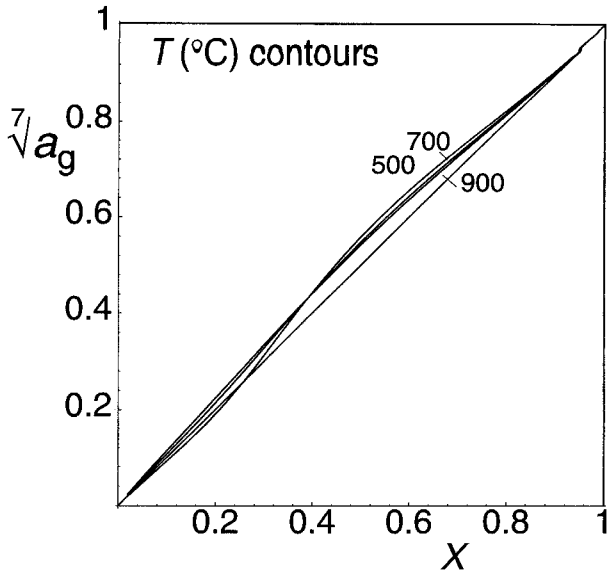

FIGURE 15. Calculated activity-composition relationships for cummingtonite-grunerite at a series of temperatures, in terms of the seventh root of the activity of grunerite. A 1:1 line corresponds to ideal mixing; in this temperature range, cummingtonite-grunerite is only slightly positively nonideal.

$$A = \Delta H_R + 7W_{cd} - 2W_{cg}$$
$$B = \frac{20}{7}W_{cg} - 10W_{cd} - 4W_{gd}$$
$$C = 7W_{gd} - 7W_{cd} - 3W_{cg}. \quad (15)$$

Regression to minimize residuals in Q for the site-distribution data yields $A = -173$, $B = -51$ kJ, and $C = 0$ for Equation 4. One further constraint is required to fix all the parameters of the model, and again the magnitude for the Fe-Mg interaction parameter per octahedral site is assumed to be 4.5 kJ. Thus, $W_{gd} = 5W_{M123} = 22.5$ kJ, which allows the determination of the remaining parameters from Equation 15: $\Delta H_R = -145.7$, $W_{cg} = 37.0$, and $W_{cd} = 6.7$ kJ.

This model is used to generate a pressure-temperature pseudosection for a fixed bulk composition representing a metamorphosed ironstone in the system FeO-MgO-SiO_2 (Fig. 16). In this diagram, which has been drawn for the bulk composition $SiO_2 = 66.67$, MgO = 3.33, FeO = 30.0%, a univariant reaction emerges from the FeO-SiO_2–subsystem invariant point at 9.9 kbar and 650 °C. The enthalpy of formation of the cummingtonite end-member in the current version of the Holland and Powell (1990) thermodynamic data set was constrained by the experimental data of Fonarev and Korolkov (1980) on this univariant reaction at 2.9 and 4.9 kbar. In nature, the breakdown of grunerite-bearing assemblages to assemblages containing orthopyroxene, which occurs just below the amphibolite-granulite boundary, is calculated as being close to 750 °C for such bulk compositions. This change occurs either through a narrow divariant band at pressures

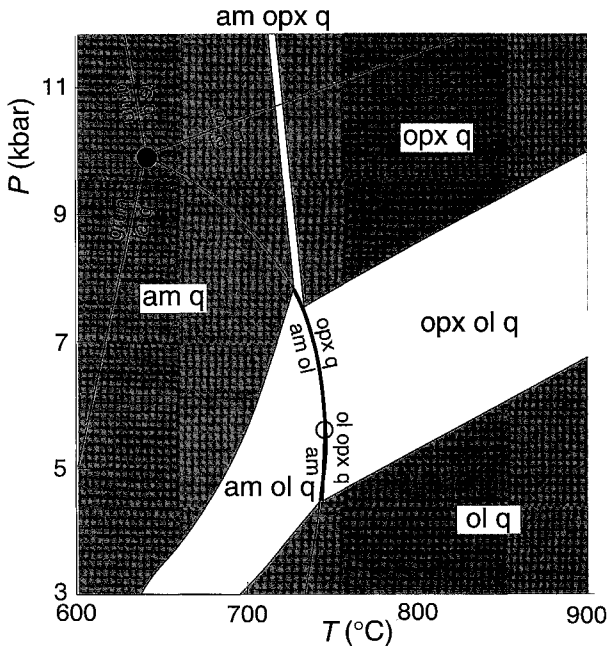

FIGURE 16. Pseudosection in FeO-MgO-SiO_2-H_2O with the phases am (ferromagnesian clinoamphibole), opx (orthopyroxene), ol (olivine), and q (quartz) involved in a univariant reaction emanating from an invariant point in FeO-SiO_2-H_2O [with fs (ferrosilite), fa (fayalite), and grun (grunerite)]. Trivariant fields are shaded, and divariant bands are white. Calculated using THERMOCALC and thermodynamic data updated from Holland and Powell (1990).

above 7 kbar or by the univariant reaction in the range 4–7 kbar.

ALKALI FELDSPAR

In contrast to the examples discussed above, in which ordering occurs at an intermediate composition in a solid solution, alkali feldspars are an example of a solid solution in which ordering occurs in both end-members of the binary (potassium and sodium feldspar). In the companion paper (Holland and Powell 1996), the ordering behavior in potassium feldspar was treated separately from that in albite, whereas the alkali feldspar join is now considered in terms of two order parameters, Q_{od} and Q_t, and one compositional parameter, X_{ab}, requiring four independent end-members in a fictive quaternary solid solution. The thermodynamics of ordering in the tetrahedral sites is modeled with the parameters from the companion paper (Holland and Powell 1996), using end-members san, orth, and mic, and the fourth end-member is chosen to be fully ordered albite ab.

The pair of equilibrium relations used to determine the two order parameters Q_{od} and Q_t are the same as used in the companion paper (Holland and Powell 1996), mic = san and orth = san. The site fractions for the tetrahedral terms are identical to those in the potassium feldspar example in that paper, and those for the alkali site are $X^A_{Na} = X_{ab}$ and $X^A_K = 1 - X_{ab}$. The potassic end-member activities are multiplied by $1 - X_{ab}$, and the ab end-member is the original mic activity multiplied by X_{ab}. The activity coefficients are given by the regular-solution expression for a quaternary among ab, san, orth, and mic. The values for all parameters are taken from the potassium feldspar model, except for the regular-solution parameters $W_{ab\ san}$, $W_{ab\ mic}$, and $W_{ab\ orth}$. Only one of these is a free parameter, the other two follow from compositional constraints coupled with the two equilibrium relations, and the value for $W_{ab\ mic}$ was chosen as 16 kJ/atom to make the crest of the alkali feldspar solvus occur near 700 °C. The resulting set of parameters is $W_{ab\ san} = 28.2$, $W_{ab\ mic} = 16$, and $W_{ab\ orth} = 24.6$ kJ.

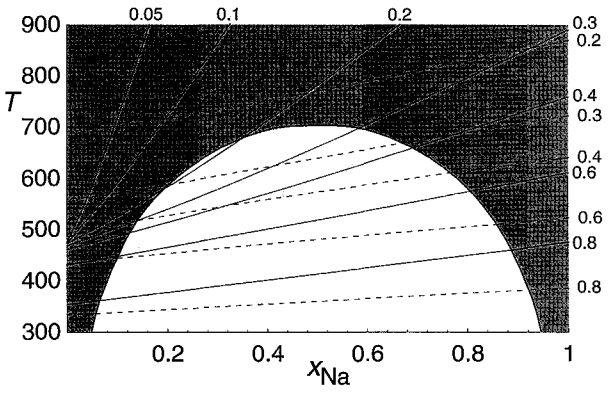

FIGURE 17. Calculated alkali feldspar T-X relations according to symmetric formalism, showing contours of Q_t and Q_{od} (see text). The solid contours refer to Q_{od}, and the dashed ones to Q_t. Calculated using THERMOCALC. T in degrees Celsius.

A calculated temperature-composition diagram is shown in Figure 17 to illustrate the variation of the two order parameters Q_{od} and Q_t with composition. The first-order behavior seen in potassium feldspar is lost almost immediately with the introduction of Na, and the phase transition becomes increasingly smeared as the degree of nonconvergence increases across the diagram toward albite. The large drop in predicted Q_{od} at the albite end occurs over the range 600–900 °C, in reasonable agreement with the studies of Goldsmith and Jenkins (1985) and Salje et al. (1985), confirming that the simple model constructed for the K end-member can make good predictions across the diagram to the Na end-member.

The symmetric solvus is an obvious effect resulting from the simple regular nature of the interactions assumed here. It is not the intention of this study to model the solvus in addition to the order-disorder relations, and a more realistic solvus could be calculated by including an asymmetric model for Na-K interactions.

DISCUSSION

Symmetric formalism is an easy to use and flexible formulation of the generalized Bragg-Williams approach to order-disorder. It is completely general in that any number of order parameters may be handled by invoking the relevant number of end-members, which are usually

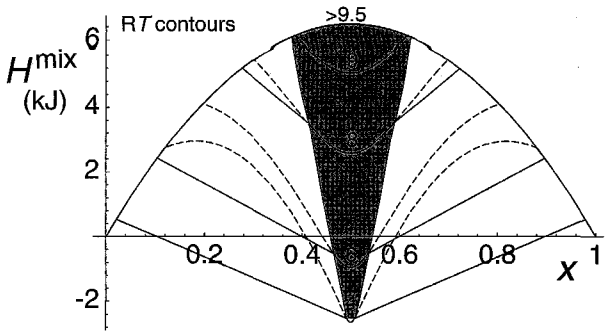

FIGURE 18. Enthalpy of mixing, H^{mix}, vs. composition, X, for the diopside-jadeite binary, contoured for RT (in kilojoules). The shaded region corresponds to the H^{mix} of the ordered phase; the solvus limbs against the ordered phase are the boundaries of this region. The calculated contours, metastable to the solvus tie lines (straight lines), are marked by dashed lines.

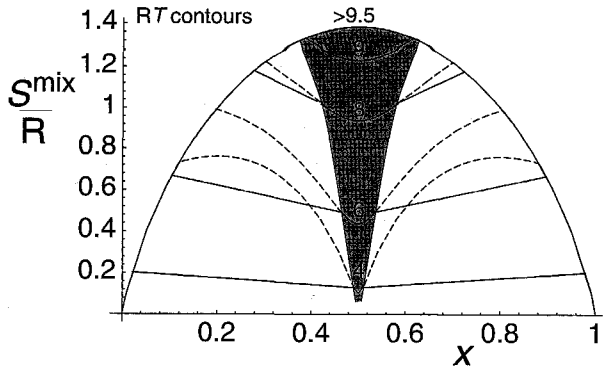

FIGURE 19. Entropy of mixing, S^{mix}/R, vs. composition, X, for the diopside-jadeite binary, contoured for RT (in kilojoules). The shaded region corresponds to the S^{mix} of the ordered phase; the solvus limbs against the ordered phase are the boundaries of this region. The calculated contours, metastable to the solvus tie lines (straight lines), are marked by dashed lines.

chosen to be ordered for algebraic simplicity. It is a simple matter to incorporate the results into an internally consistent thermodynamic data set because only the properties of the extra fictive end-members need to be introduced.

Symmetric formalism is more straightforward to use than Landau theory in dealing with solid solutions because its use of configurational entropy makes the extension to complex solid solutions involving many composition dimensions relatively simple, and because the composition dependence of the thermodynamics appears naturally. The great strength and power of Landau theory is its ability to handle nonconfigurational order-disorder effects associated with phase transitions. It can be argued that in some cation-ordering situations nonconfigurational entropy terms are important, and hence Landau theory might be more appropriate than a Bragg-Williams approach. If such terms can be shown to be significant for a particular example, symmetric formalism may be extended by making the A or B terms in Equation 4 functions of temperature, as discussed in the companion paper (Holland and Powell 1996).

Quite complex order-disorder problems can be tackled with this simple model without recourse to temperature- or pressure-dependent interaction energies. Indeed, if the interaction energies used in any model require strong temperature dependence, this may be indicating a problem with the algebraic form of the model. A regular solution for a binary cannot deal with the entropy or enthalpy changes involved when cation distributions begin to depart from the disordered case (see Figs. 18 and 19). Thus, the common assumption that a temperature-dependent interaction energy may be used to mimic the effects of cation ordering is true only for extremely small ranges of both temperature and composition.

The use of order-disorder models is indispensable for the success of both phase-equilibrium calculations and thermobarometric applications in petrology. Symmetric formalism provides a simple and effective environment for putting the thermodynamics of cation ordering into practice.

ACKNOWLEDGMENTS

Critical comments from M.S. Ghiorso and three anonymous referees are gratefully acknowledged. Dexter Perkins is particularly thanked for his patience and wise advice. Any omissions or errors are, of course, entirely our own responsibility.

REFERENCES CITED

Anderson, G.M., and Crerar, D.A. (1993) Thermodynamics in geochemistry, 588 p. Oxford, U.K.

Anovitz, L.M., Essene, E.J., and Dunham, W.R. (1988) Order-disorder experiments on orthopyroxenes: Implications for the orthopyroxene geospeedometer. American Mineralogist, 73, 1060–1073.

Besancon, J.R. (1981) Rate of cation disordering in orthopyroxenes. American Mineralogist, 66, 965–973.

Carpenter, M.A. (1980) Mechanisms of ordering and exsolution in omphacites. Contributions to Mineralogy and Petrology, 71, 289–300.

———(1981) Time-temperature-transformation (TTT) analysis of cation disordering in omphacite. Contributions to Mineralogy and Petrology, 78, 433–440.

Carpenter, M.A., Domeneghetti, M.C., and Tazzoli, V. (1990) Application of Landau theory to cation ordering in omphacite: I. Equilibrium behavior. European Journal of Mineralogy, 2, 7–18.

Carpenter, M.A., Powell, R., and Salje, E.K.H. (1994) Thermodynamics of nonconvergent cation ordering in minerals: I. An alternative approach. American Mineralogist, 79, 1053–1067.

Carpenter, M.A., and Salje, E.K.H. (1994) Thermodynamics of nonconvergent ordering in minerals: II. Spinels and the orthopyroxene solid solution. American Mineralogist, 79, 1068–1083.

Chatillon-Colinet, C., Newton, R.C., Perkins, D., III, and Kleppa, O.J. (1983) Thermochemistry of $(Fe^{2+},Mg)SiO_3$ orthopyroxene. Geochimica et Cosmochimica Acta, 47, 439–444.

Davidson, P.M., and Burton, B.P. (1987) Order-disorder in omphacitic pyroxenes: A model for coupled substitution in the point approximation. American Mineralogist, 72, 337–344.

Evans, B.W., and Ghiorso, M.S. (1995) Thermodynamics and petrology of cummingtonite. American Mineralogist, 80, 649–663.

Fonarev, V.I., and Korolkov, G.J. (1980) The assemblage orthopyroxene + cummingtonite + quartz: The low-temperature stability limit. Contributions to Mineralogy and Petrology, 73, 413–420.

Ghiorso, M.S. (1990a) Thermodynamic properties of hematite-ilmenite-geikelite solid solutions. Contributions to Mineralogy and Petrology, 104, 645–667.

———(1990b) Application of the Darken equation to mineral solid solutions with variable degrees of order-disorder. American Mineralogist, 75, 539–543.
Ghiorso, M.S., Evans, B.W., Hirschmann, M.M., and Yang, H. (1995) Thermodynamics of the amphiboles: Fe-Mg cummingtonite solid solutions. American Mineralogist, 80, 502–519.
Goldsmith, J.R., and Jenkins, D.M. (1985) The high-low albite relations revealed by reversal of degree of order at high pressures. American Mineralogist, 70, 911–923.
Grammenopoulou, S. (1981) Eigenschaften und Oxidationsbestandigkeit synthetischer Orthopyroxene. Ph.D. dissertation, Christian-Albrechts University, Kiel, Germany (not seen; extracted from American Mineralogist, 73, 1072, 1988).
Hackler, R.T., and Wood, B.J. (1989) Experimental determination of Fe and Mg exchange between garnet and olivine and estimation of Fe-Mg mixing properties in garnet. American Mineralogist, 74, 994–999.
Hirschmann, M., Evans, B.W., and Yang, H. (1994) Composition and temperature dependence of Fe-Mg ordering in cummingtonite-grunerite as determined by X-ray diffraction. American Mineralogist, 79, 862–877.
Holland, T.J.B. (1983) The experimental determination of activities in disordered and short-range ordered jadeitic pyroxenes. Contributions to Mineralogy and Petrology, 82, 214–220.
———(1990) Activities in omphacitic solid solutions: An application of Landau theory to mixtures. Contributions to Mineralogy and Petrology, 105, 446–453.
Holland, T.J.B., and Powell, R. (1990) An internally consistent thermodynamic dataset with uncertainties and correlations: The system Na_2O-K_2O-CaO-MgO-MnO-FeO-Fe_2O_3-Al_2O_3-SiO_2-TiO_2-C-H_2-O_2. Journal of Metamorphic Petrology, 8, 89–124.
———(1996) Thermodynamics of order-disorder in minerals: I. Symmetric formalism applied to minerals of fixed composition. American Mineralogist, 81, 1413–1424.
Kroger, F.A., Stieltjes, F.H., and Vink, H.J. (1959) Thermodynamics and formulation of reactions involving imperfections in solids. Phillips Research Report, 14, 557.
Kroll, H., Schlenz, H., and Phillips, M.W. (1994) Thermodynamic modelling of non-convergent ordering in orthopyroxenes: A comparison of classical and Landau approaches. Physics and Chemistry of Minerals, 21, 555–560.
Molin, G.M., Saxena, S.K., and Brizi, E. (1991) Iron-magnesium order-disorder in an orthopyroxene crystal from the Johnstown meteorite. Earth and Planetary Science Letters, 105, 260–265.
Navrotsky, A. (1971) The intracrystalline cation distribution and the thermodynamics of solid solution formation in the system $FeSiO_3$-$MgSiO_3$. American Mineralogist, 56, 201–211.
Perkins, D., and Vielzeuf, D. (1992) Experimental investigation of Fe-Mg distribution between olivine and clinopyroxene: Implications for mixing properties of Fe-Mg in clinopyroxene and garnet-clinopyroxene thermometry. American Mineralogist, 77, 774–783.
Powell, R. (1978) Equilibrium thermodynamics in petrology, 284 p. Harper and Row, New York.
———(1983) Thermodynamics of complex phases. In S.K. Saxena, Ed., Kinetics and equilibrium in mineral reactions, p. 241–266. Springer-Verlag, New York.
Powell, R., and Holland, T.J.B. (1988) An internally consistent thermodynamic dataset with uncertainties and correlations: 3. Application methods, worked examples and a computer program. Journal of Metamorphic Geology, 6, 173–204.
———(1993) On the formulation of simple mixing models for complex phases. American Mineralogist, 78, 1174–1180.
Sack, R.O. (1980) Some constraints on the thermodynamic mixing properties of Fe-Mg orthopyroxenes and olivines. Contributions to Mineralogy and Petrology, 71, 257–269.
Sack, R.O., and Ghiorso, M.S. (1994) Thermodynamics of multicomponent pyroxenes: 1. Formulation of a general model. Contributions to Mineralogy and Petrology, 71, 257–269.
Salje, E.K.H., Kuscholke, B., Wruck, B., and Kroll, H. (1985) Thermodynamics of sodium feldspar: II. Experimental results and numerical calculations. Physics and Chemistry of Minerals, 12, 99–107.
Saxena, S.K., and Ghose, S. (1971) Mg^{2+}-Fe^{2+} order-disorder and the thermodynamics of the orthopyroxene crystalline solution. American Mineralogist, 56, 532–559.
Skogby, H. (1992) Order-disorder kinetics in orthopyroxenes of ophiolite origin. Contributions to Mineralogy and Petrology, 109, 471–478.
Thompson, J.B. (1967) Thermodynamic properties of simple solutions. In P.H. Abelson, Ed., Researches in geochemistry, p. 340–361. Wiley, New York.
von Seckendorff, V., and O'Neill, H.St.C. (1993) An experimental study of Fe-Mg partitioning between olivine and orthopyroxene at 1173, 1273 and 1423 K and 1.6 GPa. Contributions to Mineralogy and Petrology, 113, 196–207.
Wiser, N.M., and Wood, B.J. (1991) Experimental determination of activities in Fe-Mg olivine at 1400 K. Contributions to Mineralogy and Petrology, 108, 146–153.
Wood, B.J., and Banno, S. (1973) Garnet-orthopyroxene and orthopyroxene-clinopyroxene relationships in simple and complex systems. Contributions to Mineralogy and Petrology, 42, 109–124.
Wood, B.J., Holland, T.J.B., Newton, R.C., and Kleppa, O.J. (1980) Thermochemistry of jadeite-diopside pyroxenes. Geochimica et Cosmochimica Acta, 44, 1363–1371.
Yang, H., and Ghose, S. (1994) In-situ Fe-Mg order-disorder studies and thermodynamic properties of orthopyroxene $(Mg,Fe)_2Si_2O_6$. American Mineralogist, 79, 633–643.

Manuscript received April 28, 1995
Manuscript accepted July 8, 1996

Appendix 1

A phase with order-disorder can be described in terms of n bulk-composition parameters, X (of which $n - 1$ are independent because $X_n = 1 - \Sigma_{i=1}^{n-1} X_i$), and s order parameters, Q. Macroscopically, such a phase is considered in terms of n (macroscopic) end-members, whereas in symmetric formalism the phase is considered in terms of $n + s$ microscopic, or fictive, end-members. In the same way that the n macroscopic end-members form an independent set of end-members sufficient to describe any (macroscopic) composition of the phase, the $n + s$ end-members of the phase form an independent set of end-members sufficient to describe any microscopic state of the phase. The logic in this appendix follows from that of Appendix 1 in the companion paper (Holland and Powell 1996).

The virtual Gibbs energy is a function of the bulk-composition parameters, X, and order parameters, Q (Kroger et al. 1959; Powell 1983). It includes both non-equilibrium and equilibrium states of the phase; the equilibrium state of the phase, Q_{equil}, is found from

$$\left(\frac{\partial G^*}{\partial Q_k}\right)_{X, Q_{j(j\neq k)}} = 0 \quad \text{for} \quad (k = 1, 2, \ldots, s). \qquad \text{(A1-1)}$$

The Gibbs energy for the equilibrium state of the phase, G, is found by substituting Q_{equil} into the expression for G^*, so $G = \{G^*\}_{Q=Q_{equil}}$. The chemical potentials of the macroscopic end-members are related to the Gibbs energy, G, by

$$\mu_K = \left(\frac{\partial NG}{\partial N_K}\right)_{N_{J(J\neq K)}} \qquad \text{(A1-2)}$$

in which N_K is the number of moles of the macroscopic

end-member, K; G is taken to be a molar quantity, so it is multiplied by N, with $N = \Sigma_{i=1}^{n} N_i$.

The (virtual) chemical potentials, μ_k^*, of the model end-members are related to the virtual Gibbs energy, G^*, by

$$\mu_k^* = \left(\frac{\partial NG^*}{\partial n_k}\right)_{n_{j(j\neq k)}} \quad \text{(A1-3)}$$

in which n_k is the number of moles of the model end-member, k, and G^* is a molar quantity multiplied by N, with $N = \Sigma_{i=1}^{n+s} n_i$.

The chemical potentials of the macroscopic end-members are a particular linear combination of the chemical potentials of the model end-members, Equation A1-3, and the main purpose of this appendix is to derive this relationship. This is important because in general the chemical potentials of the model end-members are particularly simple to write [for example, with symmetric formalism, Powell and Holland (1993)].

To generate the chemical potential of a macroscopic end-member, μK, the starting point is the definition, Equation A1-2, and application of the chain rule:

$$\mu_K = \left[\sum_{j=1}^{n+s}\left(\frac{\partial NG^*}{\partial n_j}\right)_{Q,n_{l(j\neq l)}}\left(\frac{\partial n_j}{\partial N_K}\right)_{Q,N_{J(J\neq K)}} + \sum_{i=1}^{s}\left(\frac{\partial NG^*}{\partial Q_i}\right)_{N_J,Q_{j(j\neq i)}}\left(\frac{\partial Q_i}{\partial N_K}\right)_{N_{J(J\neq K)}}\right]_{Q=Q_{equil}}. \quad \text{(A1-4)}$$

From using Equations A1-1 and A1-3 in Equation A1-4, it follows that

$$\mu_K = \sum_{i=1}^{n+s}\{\mu_i^*\}_{Q=Q_{equil}}\left(\frac{\partial n_i}{\partial N_K}\right)_{N_{J(J\neq K)},Q}. \quad \text{(A1-5)}$$

Thus, Equation A1-5 allows the chemical potentials of the macroscopic end-members to be written in terms of the virtual chemical potentials of the model end-members. In many simpler cases $\mu_K = \{\mu_k^*\}_{Q=Q_{equil}}$, where K has the same composition as k.

Obtaining the equilibrium values of Q to substitute into the μ_i^* in Equation A1-5 involves using Equation A1-1. This is accomplished most simply by using

$$\left(\frac{\partial G^*}{\partial Q_k}\right)_{Q_{j(j\neq k)}} = \sum_{j=1}^{1+s}\left(\frac{\partial p_j}{\partial Q_j}\right)_{Q_{l(l\neq j)}}\mu_i^* = 0 \quad \text{(A1-6)}$$

for each Q_k, following Appendix 1 of Holland and Powell (1996). The sum in Equation A1-6 for each Q_k is equivalent to an equilibrium relationship for a balanced reaction between the model end-members:

$$\sum_{i=1}^{n+s} r_{ki}\mu_i^* = 0 \quad \text{for} \quad (k = 1, 2, \ldots, s) \quad \text{(A1-7)}$$

where r_{ki} are the reaction coefficients for the kth reaction. Although many reactions can be written between the model end-members, there are only s independent ones. This equation is more convenient for formulating the equilibrium conditions than using Equation A1-1 directly, particularly if the virtual chemical potentials are simple to formulate.

If a general expression is needed for the virtual chemical potentials, then, starting with Equation A1-3 and using the chain rule gives

$$\mu_k^* = G^* + \sum_{i=1}^{n-1} N\left(\frac{\partial G^*}{\partial X_i}\right)_{X_{l(l\neq i)},Q_j}\left(\frac{\partial X_i}{\partial n_k}\right)_{n_{j(j\neq k)}} + \sum_{i=1}^{s} N\left(\frac{\partial G^*}{\partial Q_i}\right)_{Q_{j(j\neq i)},X_l}\left(\frac{\partial Q_i}{\partial n_k}\right)_{n_{j(j\neq k)}}. \quad \text{(A1-8)}$$

Formulating G^* in terms of X and Q gives a straightforward way of generating the virtual chemical potentials. This equation, in combination with Equation A1-5, gives the chemical potentials of the macroscopic end-members. Note that Equation A1-8 is identical to the equations of Ghiorso (1990a, 1990b) without recourse to Darken's equation, observing that he delivered equations for the virtual chemical potentials (in the notation used here). Note that the last sum in Equation A1-8 is equal to zero through Equation A1-1, if Equation A1-8 is to be used only in an equilibrium context.

Appendix 2

The mixing properties of solid solutions are also well handled by symmetric formalism, and these relationships are outlined here for the two-site mixing case, with the site proportion $m:n$.

The Gibbs energy of the solid solution is given by the expression for a ternary regular solution, in terms of the proportions of the three end-members:

$$G_{ss} = p_aG_a + p_bG_b + p_oG_o + p_ap_bW_{ab} + p_op_aW_{ao} + p_op_bW_{bo} - TS_{mix}. \quad \text{(A2-1)}$$

The excess Gibbs energy of mixing is found from

$$G_{ex} = G_{ss} + TS_{mix} - XG_b - (1 - X)G_a = \frac{1}{m+n}\left[(A + CX)Q + \frac{B}{2}Q^2\right] + W_{ab}X(1 - X)$$

in which A, B, and C are from Equation 4. If, as used here, the constituent parts of A, B, and C are independent of temperature, then the enthalpy of mixing is given by

$$H_{mix} = \frac{1}{m+n}\left[(A + CX)Q + \frac{B}{2}Q^2\right] + W_{ab}X(1 - X). \quad \text{(A2-2)}$$

The compositional dependence of the enthalpy of mixing at several temperatures for omphacite is shown in Figure 18. The relationships are limited by the high-temperature disordered behavior, which gives the familiar regular-solution parabolic curve increasing to a maximum at $X = 0.5$. At lower temperatures, the enthalpy of ordering causes the mixing enthalpy to depart to more negative values from the disordered limit, with the effect becoming larger as $X = 0.5$ is approached. This leads to a progressive enthalpic stabilization of the ordered omphacite as temperature is reduced. With suitable choices

of parameters the enthalpy of mixing can be positive near the ends of the binary join but negative near the center.

For the same assumption of independence with respect to temperature as used above in Equation A2-2, the entropy of mixing is given by

$$S_{mix} = -R\left[m\left(1 - X + \frac{n}{m+n}Q\right)\ln\left(1 - X + \frac{n}{m+n}Q\right) + m\left(X - \frac{n}{m+n}Q\right)\ln\left(X - \frac{n}{m+n}Q\right) + n\left(X + \frac{m}{m+n}Q\right)\ln\left(X + \frac{m}{m+n}Q\right) + n\left(1 - X - \frac{m}{m+n}Q\right)\ln\left(1 - X - \frac{m}{m+n}Q\right)\right]. \quad \text{(A2-3)}$$

If the constituent parts of A, B, and C are a function of temperature, then the terms in Equation A2-2 are the constant parts, and in Equation A2-3 additional terms of the form of Equation A2-2 involving the temperature derivatives of A, B, C, and W_{ab} occur.

The entropy of mixing as a function of composition at various temperatures is shown in Figure 19. It is bounded by the maximum disordered entropy at high temperatures. The behavior is very similar to the enthalpy of mixing seen in Figure 18, except that the minimum at $X = 0.5$ at very low temperatures does not become negative (unless the ordered intermediate end-member has a negative vibrational excess entropy or some other negative nonconfigurational contribution).

Heat capacities are found from the relation

$$C_P = \left(\frac{\partial H}{\partial T}\right)_X = \left(\frac{\partial H}{\partial T}\right)_{Q,X} + \left(\frac{\partial H}{\partial Q}\right)_{T,X}\left(\frac{\partial Q}{\partial T}\right)_X. \quad \text{(A2-4)}$$

The heat capacity of omphacite as a function of temperature at different compositions is shown in Appendix Figure 1, calculated using Equation A2-4. The heat capacity is slightly curved at low temperatures but approaches linear behavior at high temperatures, dropping to zero at the critical temperature (Appendix Fig. 1). As composition moves away from $X = 0.5$, the maximum C_P and the critical temperature both fall.

If any terms in Equation 4 are pressure dependent, then the volume of mixing has the same form as Equation A2-2, involving the pressure derivatives of A, B, C, and W_{ab}. It is reasonable to consider that the volume of mixing is zero unless a case can be made for the ordered end-member having a volume different from the average of the two binary end-members, as might occur if lattice strains on ordering lead to an excess volume (at $X = 0.5$). In general, all the Ws are expected to be pressure independent, except for W_{ab}, which is the usual regular term for excess volumes of mixing in disordered solutions.

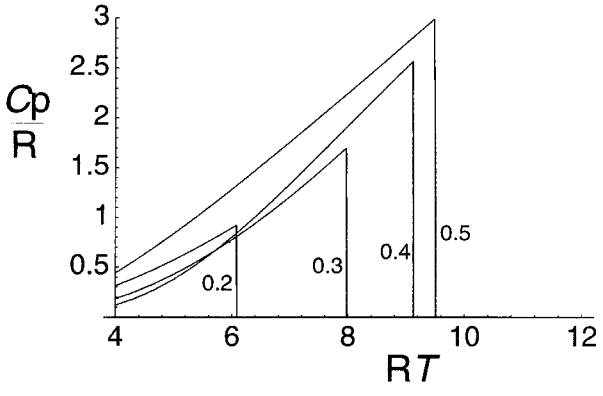

Appendix Figure 1. Heat capacity of mixing, C_P^{mix}/R, vs. RT (in kilojoules) for the diopside-jadeite binary, contoured for X.